3D Statistical Parametric Mapping of EEG Source Spectra by Means of Variable Resolution Electromagnetic Tomography (VARETA)

J. Bosch-Bayard, P. Valdés-Sosa, T. Virues-Alba, E. Aubert-Vázquez, E. Roy John, Thalia Harmony, J. Riera-Díaz and N. Trujillo-Barreto

Key Words
EEG Spectrum
Inverse Solutions
QEEG Norms
Statistical Parametric Mapping
Z Transform
VARETA

ABSTRACT

This article describes a new method for 3D QEEG tomography in the frequency domain. A variant of Statistical Parametric Mapping is presented for source log spectra. Sources are estimated by means of a Discrete Spline EEG inverse solution known as Variable Resolution Electromagnetic Tomography (VARETA). Anatomical constraints are incorporated by the use of the Montreal Neurological Institute (MNI) probabilistic brain atlas. Efficient methods are developed for frequency domain VARETA in order to estimate the source spectra for the set of 10^3-10^5 voxels that comprise an EEG/MEG inverse solution. High resolution source Z spectra are then defined with respect to the age dependent mean and standard deviations of each voxel, which are summarized as regression equations calculated from the Cuban EEG normative database. The statistical issues invoked are addressed by the use of extreme value statistics. Examples are shown that. illustrate the potential clinical utility of the methods herein developed.

INTRODUCTION

me quantitative evaluation of the frequency content of EEG b&ground activity has been the focus of intense research activity for several decades.[1-3] Though other aspects of EEG activity may be measured,' quantitative electroencephalography (QEEG) has been, to date, almost exclusively based upon spectral analysis.

The seminal work by Matousek and Petersen (1973) showed the age dependence of broad band EEG spectral parameters (BBSP) and the possibility of constructing age corrected tables of these measurements to highlight pathology. Subsequent work by John et al (1980)[6] established the use of both a) regression equation of QEEG parameters with age ("developmental equations") to partial out the variation due to normal brain maturation, and b) the Z transform, to quantify the deviation from normality. This work also underscored the importance of log transforming BBSP to conform to the requirements of parametric statistics. Shortly thereafter, Duffy et al (1981)[7] introduced the technique of Statistical Probability Mapping and the idea that mapping of statistics derived from EEG and EP signals could help to localize brain abnormalities. The increase of diagnostic accuracy accruing from use of these procedures was discussed in John et al. (1988).[8] Subsequently, the use of developmental equations was shown valid for sub jects from Cuba[9] and from many different cultures.

Assessments of this technique have documented its present utility in many clinical applications. A number of classification algorithms based upon QEEG have been described. The area 'A' under the Receiver Operating Curve (ROC) assessed the diagnostic accuracy of a specific set of BBSP. The ROC curve is a plot of True Positive probability vs. False Positive probability,[10] and varied from a chance level for some disease entities to more than 0.8 in tumors and epilepsy." The major recent developments of QEEG have been directed toward increasing its sensitivity and specificity for the detection of abnormal background rhythms, especially for classification of major categories of neuro-psychiatric diseases (see review in Hughes and John, 1999).[12]

High, independently replicated specificity and sensitivity of multiple discriminant functions has been demonstrated for differential classifications of a number of different neuro-psychiatric pathologies. Cluster analyses based upon QEEG measures have revealed the existence of heterogeneous pathophysiological subtypes within symptomatically homogeneous samples of patients, with differen-

From the Laboratory of Neurosciences, Cuban National Scientific Research Center, Havana, Cuba. E. Roy John PhD, is from the Brain Research Laboratories, Department of Psychiatry, New York University School of Medicine and the Nathan S. Kline Institute for Psychiatric Research, Orangeburg, N.Y. Thalia Harmony, M.D. from the Center of Neurobiology, National Autonomous University of Mexico (UNAM), Mexico.

Address correspondence to Dr. J. Bosch-Bayard: bosch@cneuro.edu.cu.

Requests for reprints should go to Dr. E. Roy John, Brain Research Laboratories, Department of Psychiatry, New York University School of Medicine, 550 First Ave., New York, NY 10016.

tial response to treatment or evolution of illness, and for identification of subtypes predictive of differential evolution or response to treatments.[13-18]

Further improvements in diagnostic accuracy were obtained by the use of the full EEG spectrum. In High-Resolution QEEG,[19] the means and standard deviations of the log spectrum are summarized as "developmental surfaces" that are a function both of age and frequency, The Z transform of the log spectrum (Z spectrum) is then a narrow band counterpart to similar BBSP measures, though the number of variables to evaluate increases and special statistical techniques are needed to control the type I error." Using ROC analysis,[21] showed that the use of the full log spectrum may increase the value of A up to 16% for some pathologies when compared to BBSP.

In spite of these promising results for the *detection* of abnormal background atiiity, the general opinion has been that traditional or Topographic OEEG has very little to *offer* in terms of *localization* of underlying pathology. This impression was corroborated in a study by Biscay et al (1992)" in which Localization Operator Curves (LOC), the *localization* problem *analogues* for ROC curves, were *introduced.* LOC curves graph measures of False Positive and False Negative pixels, weighted in accordance to their distances from the true localization of the lesion and the region detected as abnormal by the classifier. LOC analysis showed that the localizing ability of QEEG parameters obtained from the raw EEG was quite limited, even when transformations such as multiiariate QEEG maps[20] or the Laplacian[23] montaage are used.

The basic difficulty is that the events of real interest to clinical neurophysiology are the primary currents of neuronal ensembles in the *brain, which* are *unobservable.* The *measurements* that are available to topographic QEEG are voltage or magnetic measurements on the scalp. It is clear that the activity recorded at each sensor is a linear combination of the activity of all generators due to volume conduction. Furthermore, the different tissues of the head effectively act as a spatial low pass filter[24] that imposes additional smearing. Thus, there Seems to be a basic limit tc the localization capability of topographic QEEG due to the biophysics of EEG generation. When this argument is reviewed, together with the impressive achievements of several other image modalities, it would seem that there is little possibility left for advance in terms of extracting localizing information from the EEG or MEG recordings obtained in clinical settings. .

Using spatio-temporal methods, an early demonstration that this is not the case was provided by Scherg and von Cramon (1985),[25] who decomposed the auditory evoked potential into a reduced number of source waveforms, used to provide an image of the source currents in activated regions on the human auditory cortex and, shortly thereafter, Scherg and von Cramon (1990)[26] illustrated the clinical utility of this method in patients with temporal lobe lesions. At about the same time, Lehman" and Michel (1989)[27] demonstrated that FFT data could be used for intracerebral localization of dipole sources of EEG power maps,

Intensified interest in EEG inverse methods is reflected in the increasing number of more recent publications reporting methods to estimate 30 distributions of primary current density that could explain observed brain electric and magnetic fields.[28-35] Particular impetus to such efforts was provided by the description of a method for Low Resolution Electromagnetic Tomography, or LORETA.[30] This report was shortly followed by the initial work by members of the present group on Variable Resolution Electromagnetic Tomography"" and related MEG efforts at source localization." These were the *initial* attempts to develop an EEG/MEG "Tomography" that would integrate the high temporal resolution of electrophysiological measurements with the spatial or metabolic information provided by other neuro-imaging modalities.[36]

Of particular interest are techniques for using individual or probabalistic anatomical information provided by MRI[37-40] to constrain EEG/MEG inverse solutions to the sites where primary currents might be generated. These constraints contribute to overcome the non-uniqueness of the inverse solutions. The use of EEG/MEG Tomography makes it possible to reformulate OEEG techniques in a 3D anatomic framework. Current methods for EEG/MEG Tomography allow the calculation of 'source derivations" that are estimates of the time varying activii of neural generators. This paper focuses upon spectral analysis of these source derivations as a natural extension of existing frequency domain QEEG techniques. This can be desig nated as Tomographic QEEG." The present method extends topographic QEEG to a spatially low-resolution tomographic QEEG that might be both practical and of potential clinical utility.*†

Accomplishment of such an *extension* required *reconciliation* with several realistic issues and the implementation of a number of new procedures:

*In an ordinary clinical setting, it is not feasible to obtain a high resolution MRI before each individual EEG recording. The use of statistical brain atlases[49,50,73-75] offers the possibility of incorporating probabilistic anatmoical constraints into the EEG/MEG inverse solution. The Montreal Neurological Institute (MNI) probabilistic atlas[49] is used here to constrain a Discrete Spline EEG inverse solution, known as Variable Resolution Electromagnetic Tomography, or VARETA.[31-33] Confirmation that acceptably accurate source localization is provided by the use of this Probabilistic MRI Atlas has been demonstrated by concordance of VARETA images with CT scans, in numerous individual patients with space occupying or cerebrovascular lesions by Fernandez-Bouzas et al (1997, 1998, 1999[45-47] and Prichep et al (2001).[48]

†A summarized version of the results of this paper was presented at the 14th International Congress of EEG and Clinical Neurophysiology.[34]

1. Methods are developed in this paper for frequency domain VARETA, which estimates the source spectra for each of the 10^3-10^5 voxels that comprise an EEG/MEG inverse solution. An efficient algorithm, based upon the computation of the square mot of the cross-spectral matrix,[41] is presented here.
2. High resolution source Z-spectra have been defined*' and age dependent means and standard deviations for the log spectrum of each voxel have been summarized as regression equations calculated from the Cuban normative EEG database.
3. A variant of Statistical Parametric Mapping[2] is introduced here for the first time to assess the significance of source log spectra. The statistical issues involved are solved by the use of extreme value statistics, as has been discussed in Galán et al (1994)[20] and placed upon a firm theoretical basis in Worsley et al (1995).[42] This paper is restricted to analysis based upon an eyes closed resting EEG from 19 scalp electrodes placed according to the International 10/20 System. The effect of using a larger number of electrodes will be discussed elsewhere.
4. Examples are shown that illustrate the potential clinical utility of VARETA, based upon data from only 19 leads.

METHODS

Normative PEEG data

The results to be presented below are based upon EEG recordings from normal subjects obtained from the Normative Cuban digiial EEG database." To construct this database, 276 subjects (133 male, 143 female) were randomly selected from a register of 116,000 inhabitants of different municipalities in Havana City. Using a stratified design, a sample was obtained with an age range from 5 to 97 years and a quasi-logarithmically spaced distribution (yearly from 5 to 15.9 years old; every two years from 16 to 19.9; every five years from 20 to 97). Strict cdteria for selection, which excluded 65% percent of the original population, resulted in this sample, considered "functionally healthy."

The EEG recordings from these subjects had been obtained using the MEDICID-03M system. The amplifier specifications of this system were: gain of 10000 dB, low cut at 0.5 Hz and high cut at 30 Hz, 60 Hz notch filter and a noise level of 2 mV RMS. The sampling frequency was 100 Hz. Nineteen monopolar derivations of the 10/20 system were recorded (FP1, FP2, F3, F4, C3, C4, P3, P4, O1, 02, F7, F8, T3, T4, T5, T6, Fz, Cz, Pz) using linked earlobes as a reference. The impedance of all derivations was required to be below 5 KΩ. Eye movement artifacts were monitored by use of the electro-oculogram (EOG).

Artifact free segments of 2.56-sec. duration were selected by means of visual editing by an expert electroencephalographer, who was also requested to eliminate obvious changes in state such as drowsiness. Twenty-four such segments of eyes closed (EC) EEG were collected from each subject. It has been shown that quantitative analysis of this amount of EEG yields a stable replicable set of QEEG measures.[6,15,43]

Frequency domain distributed source analysis

The source analysis in the frequency domain consists of the following steps:

First, as is usual in QEEG analysis, time domain EEG data is transformed to the frequency domain (see Appendix A). Using each frequency in every channel, the complex covariance matrix, known as the cross-spectra, is calculated. When analyzing topographic spectra, only the real values [the diagonal of the cross-spectral matrix) are used. However, as is shown in Appendix B, calculation of the source spectra for tomography requires the use of the full information, which is available in the cross-spectral matrix. This is because the tomographic inverse solution is a linear mmbinatiin of both the spectra and cross-spectra derived from the surface recording. In other words, the additional information contained in the EEG cross-spectra quantifies the inter-correlations of electrical activity among electrodes, which provides essential constraints upon potential configuration of sources.

Second, the cross-spectral matrices obtained from the surface are used to calculate the cross-spectral matrices of the sources for each frequency. To do this, it is necessary to obtain an estimate of the primary currents in the sources that generate the voltages measured in the electrodes during the EEG recording. This problem is known as the "inverse problem (IP) of electroencephalography." It is well known that the IP problem has no unique solution. A number of methods have been proposed to circumvent this difficulty. In this paper, we use the method developed by Valdes and his collaborators,[31,32] named Variable Resolution Electrical Tomography (VARETA).

VARETA is a technique for estimating the distribution of the primary current in the source generators of EEG data. Like Low Resolution Electromagnetic Tomography or LORETA,[30] VARETA is a Discrete Spliie Distributed Solution." Spline estimates are the spatially smoothest solutions compatible with the observed data. However, while LORETA imposes maximal spatial smoothness. VARETA imposes different amounts of spatial smoothness for different types of generators, the actual degree of smoothness in each voxel being determined by the data itself, hence the use of the term variable resolution. VARETA allows spatially adaptive nonlinear estimates of current sources and eliminates 'ghost solutions" (artifactual interference patterns), which are often present in lin-

*Preliminary papers describing VARETA can be found at http://www.geocities.com/CapeCanaveral/Lab/8084/

ear distributed inverse solutions.* Due to this procedure, VARETA produces focal solutions for point sources, as well as distributed solutions for diffuse sources.

Understanding this nonlinear estimation procedure requires some further comment. Bayes theorem is used whenever a *priori* constraints are necessary in a statistical estimation problem. Both LORETA and VARETA are Bayesian estimators of the primary current. While LORETA assumes a fixed "smooth" covariance matrix for the primary current, VARETA estimates the spatial covariance matrix and actually uses the results to impose voxel current gradients which best conform to its assumptions of smoothness. Together with the use of voxel Z scores (see discussion of effects of Z in Appendix B), this acts to diminish the dominance over deeper sources otherwise assigned to sources near the surface of the cortex. The effectiveness of these steps can be gauged by the apparent ability of VARETA to localize deep sources accurately.[45-48] In addition, anatomical constraints are placed upon the allowable solutions by introducing a "gray matter weight" for each voxel. The effect of these weights on the inverse solution is to prohibit sources where the mask is zero (for example, CSF or white matter). VARETA solutions are plotted in proportional Talairach space using probability masks derived from the average Probabilistic MRI Atlas produced by the Montreal Neurological Institute.[36,49-51] The mean head used in this work was obtained4 by averaging a set of 305 normal MRI scans, transformed to Talairach space after being subjected to nonlinear warping to match a set of 50 common landmarks. When a precise localization is desired, MRI scans of an individual subject can be used.

An average head volume conductor model was constructed and placed in registration with the Probabilistic MRI Atlas with the positions of the 19 electrodes in Talairach space, as has been defined in Brain Electric Source Analysis (BESA).[25] Further details of this three concentric sphere model have been described elsewhere.' The version of VARETA in previous descriptions,[31-33,53,54] was developed for the time domain. In this paper, we extend this methodology to the frequency domain. For those readers interested in the mathematical aspects, a detailed description of this procedure is provided in Appendix B. The most outstanding feature of this implementation is that the cross-spectral matrices in the sources are obtained directly from the cross-spectral matrices in the surface. This greatly facilitates the computation.

QEEG for source spectra (QEEGT)

The methodology developed for the quantitative analysis of the EEG (QEEG) at the scalp electrodes has ken extended here to the sources. Two major steps were required:

a) Previous studies[2,3,6,8,15,19,55-57] have shown that the logarithmic transform ensures approximate Gaussianity both for broad band as well as narrow band absolute power spectral parameters. Following this approach a regression model was fitted for the full set of frequencies and all voxels. (See Equation (9) in Appendix B). Therefore, age regression equations were calculated for the source spectra for the full frequency range, from a database of normal subjects. Evaluating these equations for every 0.39 Hz narrow band across the frequency range 0.39 to 19 Hz and the age range (5 to 97 years) of the normative database, 3D surfaces of the evolution of the EEG spectra for each source were obtained.

b) The techniques that have been developed by Valdés et al (1990, 1992)[19,58] for the statistical parametric mapping of lhe log spectra calculated from scalp recordings were now extended to the analysis of source spectra. In order to evaluate the statistical probability of any voxel value at any frequency, it is necessary to compare the log transformed source spectra with age matched normative values for the corresponding voxel. This transformation was initially introduced by John et al. (1977)[2] to achieve a known standard distribution for al QEEG variables. To achieve similar known distributions for values to be used in VARETA, we have defined the Z transform for the source spectrum (Equation (10) in Appendix B). This permits the calculation of Me Z transform for every voxel at every frequency, relative to the age expected normatie values. The result yields a 3D image of Z values for all the sources at each frequency, which can be viewed as a statistical pobabilii tomographic image, with each voxel color-coded proportional to its Z score.

Use of the Z-transform not only provides an objective criterion for estimation of statistical significance, but also confers an additional major benefit. Rescaling each voxel at each frequency to Z-values, in conjunction with the use of variable rather than fixed resolution and the spatial constraints provided by use of a probabilistic mask restricting swrces to gray matter, acts to diminish the relative contributions to VARETA images from swrces close to the surface. Without this mitigating modification, sources near the cortical surface would dominate the images and effectively mask the detection of deep-lying sources (Equation (6) in Appendix B shows another way to deal with such domination by the more superficial sources). The effectiveness of Z transform in this regard will be illustrated by simulations in a subsequent paper.

Z values may be displayed either:

- as a function of frequency (Z source spectra) at a given voxel, or
- as a function of selected tomographic slices (Z image) spaced at intervals which correspond to the slices in the Talairach atlas (depending upon the orientation of the slices, the interval between them varies from about 4 to 17 mm).

Special purpose 3D graphic tools were developed in order to allow such interactive evaluation of the large

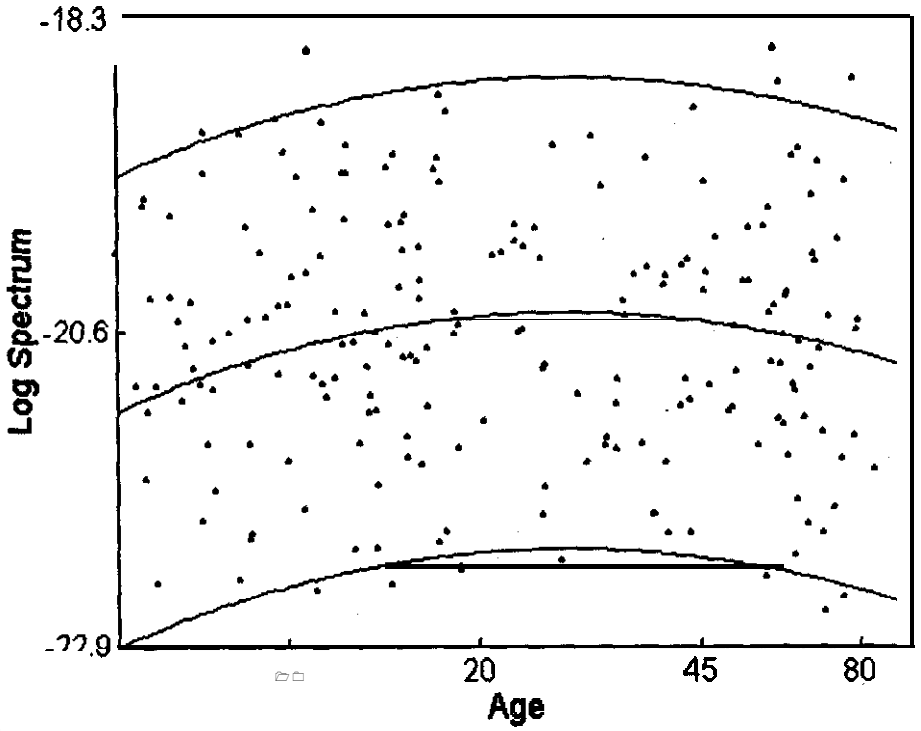

Figure1 .
Scatter plot of me source spectrum with age. Vertical axis: the spectrum at frequency 9.75 Hz for a voxel near the calcarine sulcus. Horizontal axis: age. The thick lines are the regression curve and the 95% confidence intervals for the data.

amount of transformed data that is available. The tomographic slices can be scanned rapidly, in the transaxial, coronal or sagittal planes. Alternatively, should it be desirable, a brain electrical tomographic (BET) viewer software algorithm enables visualization of the 3D image sliced along any desired oblique plane. The anatomical identification of any selected voxel is automatically displayed, based on the probabilistic classification of brain tissues developed at MNI.

In a generalization of topographic maps, three-dimensional color-coded images are generated, in which every voxel is color-coded, scaled in units of standard deviations. This quantifies the significance of the deviation of a given voxel from the corresponding age matched normative group. Extreme deviations from the normative values will show up as "hot spots" as has become standard in Statistical Parametric Mapping (SPM).

As with other variants of SPM, an important issue is the correct assessment of the probability of deviations from the norms. This must take into consideration the large number of measurements and their correlation.[20] In this work, the approach introduced by Worsley et al (1995)[42] is taken. This author uses the theory of Gaussian random fields to compute the probability of the maxima or minima of image data. Thii probability depends on the shape of the search region as well as on the correlation between voxel values.

Regularization parameters

The source spectra for the 276 individuals in the "normative database ware analyzed for each of 49 frequencies, in steps of 0.39 Hz from 0.39 to 19 Hz, for a grid size of 3623 voxels, yielding a basic database of approximately 49 million source spectra. In order to restrict the permitted gradients from voxel to voxel and thereby specify the amount of smoothing, a "regularization parameter" (see equation (5) in Appendix B) must be calculated.

A major question was whether it was necessary to calculate the regularization parameter for each single cross-spectral matrix. The regularization parameter calculated from the raw EEG crass-spectra of the normative subjects varied considerably. However, after transformation to the average reference and rescaling to standardize the geometric power as the Global Scale Factor (see expression (3) in Appendix A), the log of the regularization parameter was well described by a Gaussian distribution with mean 0.22 and standard deviation 0.04. In view of this small value for the standard deviation, the regularization parameter was fixed to the mea" value. This accelerated the Calculations by a" order of magnitude.

RESULTS

A quadratic regression provided a" adequate fit to the data in all cases. The adequacy of the log transforms to

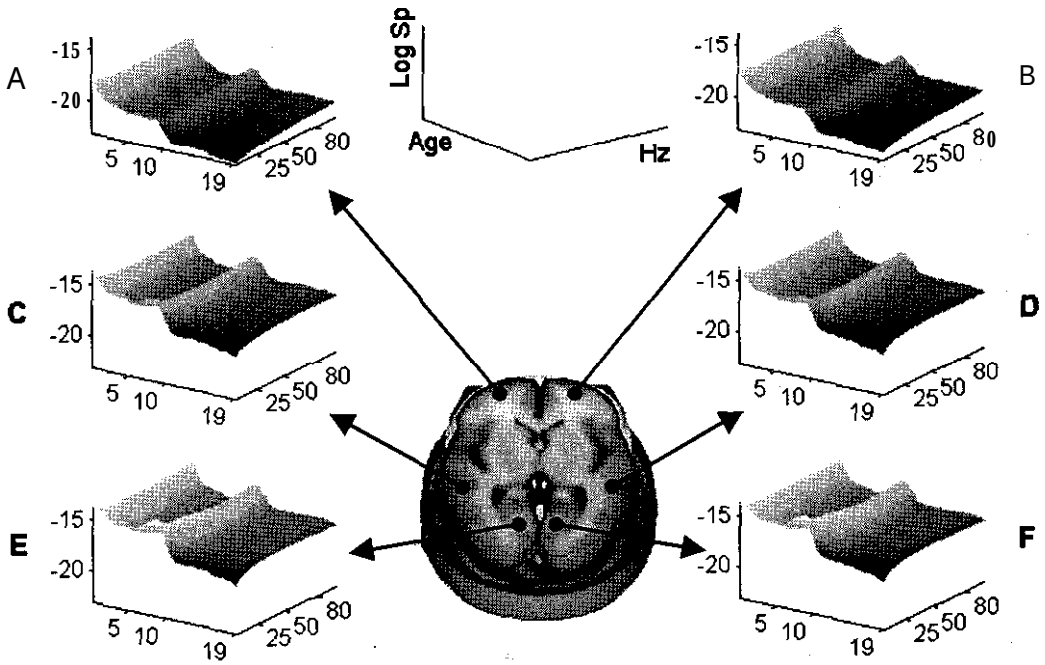

Figure 2.
Patterns of EEG source spectral maturation. The insets on the sides show the regression surfaces for the mean log source spectra of voxels from the right (A, C, E) and left (B, D, F) frontal, temporal and occipital lobes. Note symmetry of regression surfaces for homologous right-left voxels. Top inset shows axes: Z-axis is log spectrum, the x-axis is frequency (0.39 to 19 Hz) and the y-axis is age (5 to 97 years).

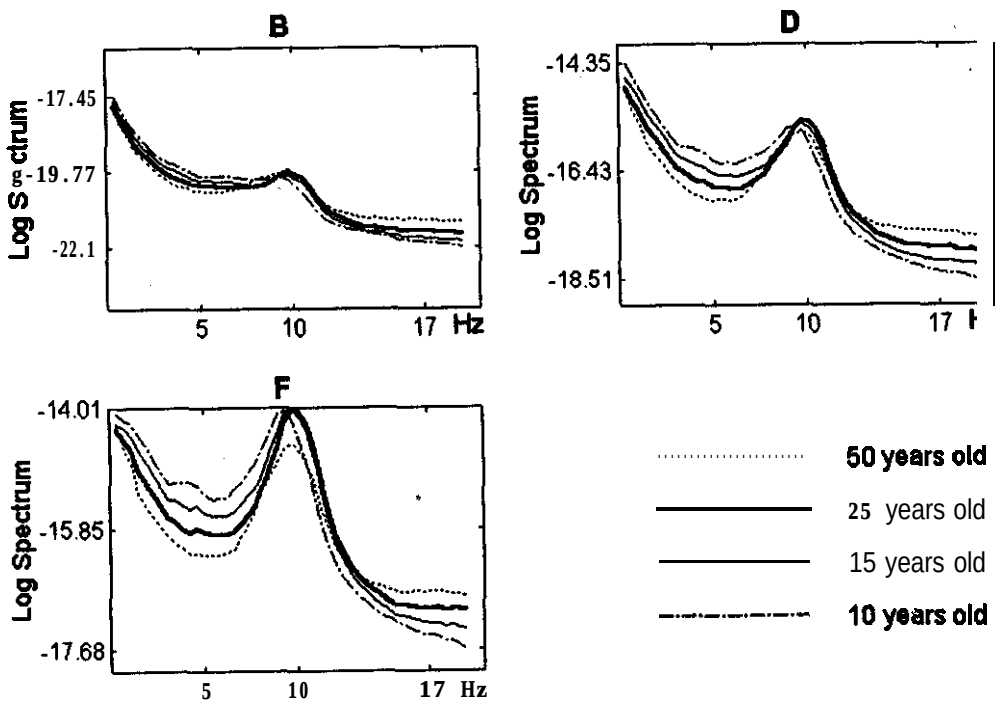

Figure 3.
Estimated mean EEG log-source spectra for ages 10, 15, 25, and 50 years for voxels indicated as B, D, and F in Figure 2.

achieve the Gaussian distributions required for valid use of parametric statistics is shown in Figure 1, which shows the scatter plot of the values of log source spectra at 9.75 Hz against age. Thii evidence was checked by means of standard goodness of fit tests for Gaussian@ The vertical axis corresponds to the log of the spectral value at this frequency for a voxel near ffie calcarine sulcus. The horizontai axis corresponds to the logarithm of age. The lines overlaid on the data points are the regression curve and the 99% confidence intervals obtained for the data.

New knowledge about the maturational changes in the QEEG was generated from the developmental surfaces. The full set of functions which define the mean value of the log spectra of the sources in each voxel, es a function of frequency and age, is the generalization of the "develop. mental equations" of John et al (1977),[2] and the "developmental surfaces" of Valdés et al (1990).[19] They describe the developmental changes of the EEG source spectrum with maturation, for every voxel within the full volume of the brain. Figure 2 shows some of these patterns of EEG source spectral maturation.

For typical voxels from the different brain lobes, this figure shows developmental surfaces in which the Z-axis is the mean value of the log spectra of the sources, the x-axis is frequency (0.39 to 19 Hz) and the y-axis is age (5 to 97 years). The symmetry of the surfaces for homologous right-left regions of the brain is striking. The main features of this surface are similar to those described previously for topographic High Resolution QEEG.[21] A peak in the alpha band is superimposed on a l/l type spectral component. The alpha peak increases in height and frequency with maturation and then slows at the upper age limit. This peak is well localized in space and frequency and shows a clear anterior-posterior gradient, being most prominent near the calcarine sulcus.

These features can be seen more clearly in Figure 3, which shows the mean EEG log-source spectra for ages 10, 15, 25, and 50 years, for the voxels designated as B, D, and F in Figure 2. Note that the scales for Figures 3 B, D, and F are logarithmic and not equal. In fact, the spectrum plotted in F is much larger than that in B.

Figure 4 presents a number of examples intended to illustrate some of the features and advantages provided by VARETA, as well as to demonstrate the accuracy of spatial localization and clinical sensitivity of Statistical Parametric Mapping of source spectra. The frequency selected for the illustration of the utility of VARETA images for basic and clinical investigations was either at the maximum value of the topographic power or at the most abnormal point in the Z-spectra of each example. A full description of each element of Figure 4 is provided in the legends of Panels A-E:

In brief, Panel A illustrates the utility of VARETA images to deblur the excessively diffuse and often misleadingly widespread distribution of activity seen at the scalp level, produced by distance from the source and the smearing influences of the scalp, skull, cerebrospinal fluid and meninges. In this Panel, QEEG topographic (a] and VARETA tomographic images (b) can be compared, as they were computed from the same eyes closed resting EEG data of one individual. The predominant and asymmetrical alpha sources are lateralized to the left side in both images. It has elsewhere been shown[32] that, depending on their directional orientation, the tomographic map may reveal lateralization of the strongest sources either ipsilateral or contralateral to the predominant location of activity in the topographic map. The VARETA image (c) from the same subject and at the same frequency, but computed from the eyes open EEG. Note the diminution of power that corresponds to alpha blocking. A quantitative study of alpha sources and their desynchronization is under preparation.

Panel B (ad) demonstrates the utility of Z-transforma-Eon of every voxel in the source spectra. It presents a) the raw VARETA image from a patient who presented with right hemiparesis and aphasia and b) the comparable VARETA image averaged across a group of healthy 76-year-olds from the Cuban normative database. The raw difference (c) between the VARETA images of the patient and the normal group and (d) the Statistical Probability VARETA Z-Image are shown, to illustrate the improved localization of abnormality obtained by replacing the raw data in each voxel by the color coded value of the corresponding Z-score computed for that frequency in that voxel.

Panel C illustrates the neuroanatomical locus of the space occupying mass parietal meningioma found in the CT of the same patient whose VARETA data ware shown in Panel B. The multimodal congruence of the lesion seen in the VARETA and CT images is apparent. Similar good neuroanatomical correspondence has been described in other radiological investigations of the utility of VARETA for localization of space occupying brain lesions.[45,46]

Panel D permits comparison of CT and VARETA localization of a cerebrovascular lesion in another patient, who presented with a left hemiparesis, right facial palsy and dysarthria. As can be seen, the CT scan from this patient revealed a hemorrhagic stroke in the right putamen and the VARETA Statistical Probability Image showed an abnormality centered upon this brain region.

Panel E illustrates findings in a patient who presented with a left hemiparesis. Clinical recovery was complete after 15 days, indicating a reversible ischemic neurological deficit, or RIND. While a CT scan (not shown) within the first 24 hours was negative, a SPECT scan carded out in the same time period (brought into registration with the average head of the probabilistic brain atlas to construct the illustrated 3D image) suggested an occlusion of the anterior branch of the right middle cerebral artery. The interpolated topographic QEEG Statistical Probability Map

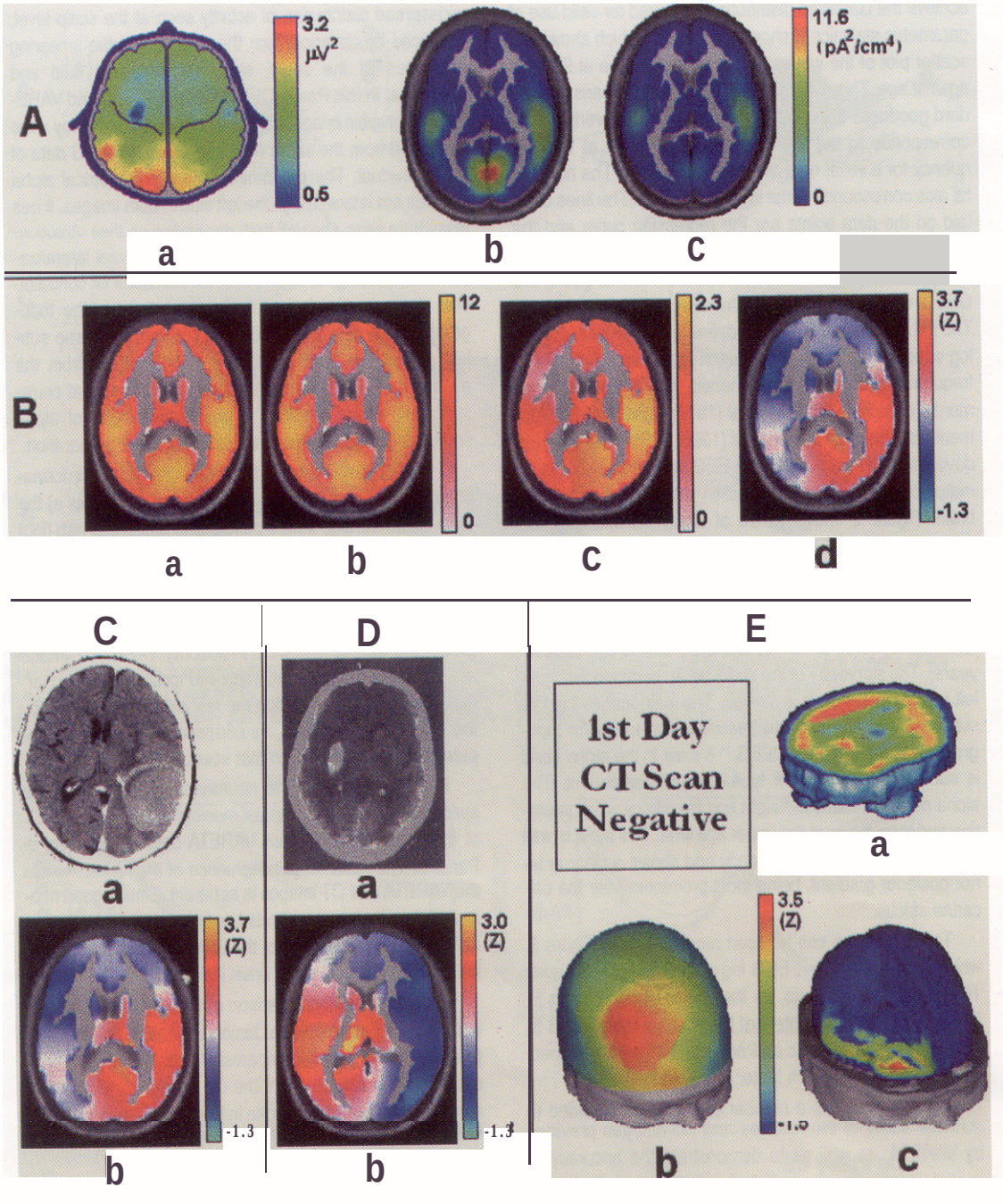

Figure 4
(See caption on facing page.)

Figure 4.

NOTE: In the QEEG image in Panel A (a) and in Panel E (a. b, c) of this Figure, tie RIGHT side of the head is displayed on the RIGHT side of the topographic image. However, radiologic convention was used in Panels B, C and D, and the LEFT side of the brain is depicted on the RIGHT side of the tomographic VARETA and CT images.

Panel A (a-c; left to right):

a) Topographic map (viewed from above with tie face at the top of the map, 19 channel eyes dosed, resting EEG recording) of absolute power (μV^2) at the peak of the Alpha band (9.75 Hz). from a normal 25-year-old male subject.

b) VARETA tomographic image of the source log absolute Alpha power ($\log \mu V^2$) at the corresponding peak (9.75 Hz). recorded from the same normal individual (eyes dosed, resting EEG recording). In this and all other VARETA images depicted in this color plate, the view is from below or in front so the left hemisphere is on the right side of ma image and sources are located in accordance with constraints provided by the MNI probabilistic brain atlas. Note the more focal distribution and multiple loci of alpha source generators in the tomographic image.

This tomographic inverse solution was calculated using only 19 electrodes arrayed according to the International 10/20 System.

C) VARETA tomographic image of the source log absolute Alpha power, in the same subject and at the same frequency as in b) above, bid far the eyes open resting EEG.

Panel B (a-d: left to right):

a) VARETA image of source log delta (2.73 Hz) in a 76-year-old male patient with right hemiparesis, who was aphasic.

b) VARETA image of *the average normal* source *log delta* (2.73 Hz) for *healthy 76-year-olds, computed* from *the* Cuban *normative* database.

c) VARETA image of the difference at 2.73 Hz between the 76-year-old patient and the average normal 76-year-old.

d) Statistical Probability VARETA Z-image of the patient at 2.73 Hz. For comparison with the actual CT scan of this patient, see Figure C (a).

Panel C (a, b; from top to bottom):

a) CT scan of 76-year-old male patient, shown above in Panel B, with right hemiparesis and aphasia, revealing a hypodense region reflecting edema surrounding a left parietal meningioma.

b) VARETAZ-image of this patient (same as in B, d), at the very narrow frequency band centered al 2.73 Hz showing abnormal excess activity in kn pareital region.

Panel D (a. b; from top to bottom):

a) CT scan of a 54-year-old female patient with hemiparesis, right facial palsy and dysarthria which was diagnosed as a hemorrhagic stroke in the right putamen.

b) VARETA Z-image of this patient, at the narrow frequency band centered at 1.56 Hz, showing abnormal excess activity with maximum in right putamen.

Panel E (a, b, c):

Data from a 72-year-old who presented with neurological symptoms which were eventually determined to reflect a reversible ischemic neurological deficit (RIND). A CT scan of this patient within the first 24 hours was negative and is therefore not shown. (Note mat in a, b, and c, the 3D images are viewed in diagonal orientation as if looking toward the lower right, with me right forehead nearest to me viewer and the nose at the lower right margin.)

a) Reconstruction of a SPECT study of this patient with a RIND, diagnosed as caused by an occlusion of the anterior branch of the right middle cerebral artery. Note the asymmetry of rCBF that corroborates the clinical diagnosis. This 3D image was obtained by placing the SPECT in registration with the average MNI head. The image has the same orientation as in b) and c).

b) Topographic statistical probability map showing Z scores distribution at 4.29 Hz for this patient, maximum in right anterior regions.

c) Tomographic VARETA statistical probability 3D image at 4.29 Hz for this patient, indicating a slow wave localized in the right anterior regions just anterior to the region of least rCBF in the SPECT. The abnormal region in the topographic image is much more diffuse than in the tomographic image. Note that the 3D images have been placed in normal orientation with the right side of the head on me righf side of the image, to make more clear the good correspondence between the site of occlusion identified by these two different functional imaging techniques

of this patient, obtained during the same time period, showed a highly significant but diffusely localized power excess on the anterior regions of the right hemisphere. The tomographic VARETA Statistical Probability Image was in good correspondence with Me SPECT, exhibiting a maximal Z value in a region of the brain just anterior to the zone of least rCBF shown in the SPECT study, but the abnormality was more discretely localized than in the topographic QEEG image.

DISCUSSION

This paper extends classical QEEG methodology, originally developed to provide statistical evaluation of local deviations from normative values of broadband spectral parameters for scalp derivations and their interpolated topographic mapping, to the tomographic localization within the volume of the brain of the generators of such scalp measurements. This requires determination of source derivations as obtained by EEG inverse solutions and their statistical evaluation. A particular type of EEG Distributed Inverse Solution, VARETA, is used for this purpose. VARETA is extended to the frequency domain, for the estimation of EEG source spectra and cross-spectra.

The result of applying VARETA to identify the locus of the alpha rhythm corresponds well to results obtained wing frequency domain source localization based upon equivalent dipole localization.[58,59] Surface topographic EEG maps reveal alpha rhythms extensively distributed across the scalp albeit with posterior predominance. The VARETA distributed inverse solution shows concentrated foci for the alpha rhythm and thus lends support to a localized origin for this rhythm in normal subjects.

One of the main objectives of the present paper was to describe the development of tomographic QEEG methods that could be used with conventional digital EEG recording systems and procedures. In order to enable widespread clinical utilization of VARETA, two obstacles had to be overcome: the need for a) individual high resolution MRI scans and b) for spatially dense arrays of EEG electrodes as prerequisites for achieving useful localization. The first goal was reached by using a probabilistic brain atlas in the calculation of the inverse solution instead of the individual's MRI. It is shown here, through examples, that this approximation may be sufficient in many situations in which a very precise MRI reconstruction is not essential. Our studies comparing the tomographic images of dense versus sparse arrays of scalp electrodes indicate that useful results may be obtained with the relatively small number of electrodes in the International 10/20 System.

These results should not be construed to mean that we are advocating the use of only a reduced electrode set. It is inevitable that the point spread function of the inverse solution increases as the number of electrodes decreases. The effect of spatial under sampling on EEG studies has been dealt with quite thoroughly recently from a theoretical point of view.[24] The use of a reduced electrode set should therefore be considered only a first approximation.

Neither do we wish to imply that individual radiological images are not advantageous for VARETA to provide more accurate functional localization. Provision has been made for VARETA to be computed when individual MRIs might be readily available or considered essential for the precise localization required for a particular clinical application. Nonetheless, reassuring evidence has been obtained which shows that loci of brain lesions within Me pseudo MRI tomogram obtained by VARETA localizations using Me Probabilistic MRI Atlas are in good registration with images of the same lesions obtained from CT or MRI scans of the individual patient-Abundant evidence also exists that the brain dysfunctions distinctive for cerebral ischemia, cognitive deterioration in the elderly, developmental disorders, major psychiatric illnesses and traumatic brain injury or post-concussive syndrome are anatomically extensive.[12] Thus, for many potential applications, the VARETA image may be found to provide a clinically useful "virtual functional MRI" image, readily available and cost effective.

Examples of clinical results that can be obtained by using SPM for source QEEG have been presented The analysis of the patient with a parietal meningioma illustrated the utility of the Z transformation to make more evident and provide statistical evaluation of a QEEG abnormality. The close correspondence between localization of lesions by VARETA Z images with more conventional radiological imaging methods was illustrated by comparison with CT images of this meningioma case and of a case of a hemorrhage in the putamen. The analysis of the patient with a reversible ischemic neurological deficit show a dose correspondence between the QEEG source Z image and the SPECT study. The degree to which source QEEG may serve in the evaluation of cerebrovascular disease is the subject of current quantitative evaluation by using L-ROC curves.[22] Until now, metabolic images have had to be collapsed in a somewhat arbitrary fashion to EEG electrodes in order to permit comparisons.[60] Additional evaluations of Me validity of VARETA in neurological disease have been carded out by studying local brain lesions and some examples have been shown elsewhere.[""]

Studies by means of simulations have demonstrated that a variable resolution inverse solution possesses certain advantages over a fixed resolution method..* Specifically, VARETA seems to eliminate ghost solutions and minimize the diffuse allocation of variance especially in the case of multiple or distributed sources.

A quantitative description of the age development of EEG source spectra has also been constructed. The resulting tomographic norms constitute a 3 dimensional extension of previous topographic normative description.[21] They also serve as the basis for construction of Statistical Parametric Maps (SPM) for source QEEG.

Obviously, further work is needed to establish the kinds of errors that might be introduced by using the average MRI atlas and the level of accuracy of spatial resolution required for useful clinical results to be provided by this method. Multimodal registration of VARETA images with other modalities of functional brain imaging in a variety of Main dysfunctions can be expected to provide important estimates of the reliability of this technique for source localization. A vexing question is the issue of what source of information could be considered as the "gold standard." Should the same gold standard be relied upon, for example, in applications as diverse as localizing the discrete brain structures occupied by a tumor or containing an epileptic focus or identifying the multiple regions and interactions possibly responsible for the behavioral and cognitive dysfunctions in a psychiatric patient, for which no reliable imaging technique has been established? How might one distinguish between a cause versus a correlate of a" abnormal brain state?

Many improvements to or extensions of the method are possible and some of them are being currently evaluated:

1. Though based upon VARETA, the SPM principles underlying tomographic QEEG are equally applicable for any type of inverse technique currently available or to be developed [e.g., Grave de Peralta et al (1996, 1997)].[61,62]
2. The probabilistic atlases used were those available. These atlases were not designed specifically for constraining EEG inverse solutions. The development of statistical atlases designed for EEG studies is being evaluated.
3. A possible problem with a probabilistic atlas might be the presence of gross brain deformations. Methods must be developed in order to deal with this situation.
4. Studies are under way to develop normative equations for a full 120-channel normative QEEG database.
5. Though possible to compute, Z images of coherence for EEG sources present a daunting problem in scientific data visualization. It is, however, the analysis of the interactions between brain regions, which is potentially the most promising area of future development of source QEEG.
6. Finally, the use of information from other neuroimaging modalities may be combined with the EEG inverse solution, in order to provide a multimodal. integrated statistical parametric map that could provide a" enhanced view of normal and pathological brain function.

ACKNOWLEDGMENTS

We would like to thank Or. Alan Evans of the International Consortium for Brain Mapping (ICBM) for provision of the probabilistic tissue maps used. This paper would not have been possible without the continual input and discussion provided by Or. Antonio Fernández-Bouzas from the Center of Neurobiology, National Autonomous University of Mexico (UNAM), Mexico and Or. Terence Picton from the Rotman Center, University of Toronto, Canada

APPENDIX A

It is well established that quantitative analysis of a total of 60 seconds artifact free EEG is sufficient to obtain stationary spectral estimates. Therefore, a total of 24 artifact-free epochs, each 2.56 seconds long, were selected. Each epoch was considered to be a time series that comprises N_d=19 components, one for each derivation. For each given time instant t, this raw EEG can be represented by a vector denoted as, $\mathbf{V}^{raw}_{i,j}$ (t), where i varies from 1 to N_s (Number of subjects), j front t to N_e= 24 (Number of EEG epochs), and t varies from 1 to N_t=256 (Number of time instants).

Transformation to the frequency **domain**

In thii method, it is assumed that the observed EEG epoch $\mathbf{V}^{raw}_{i,j}$ (t), results from distortions of the "true" EEG activity $\mathbf{V}_{i,j}(t)$ by two influences: a) the first one arises from attenuation of the raw EEG by variability of scalp and skull thickness, changes in conductivity between the brain and the surface related to age and other factors; b) the contribution of the reference activity, whii has been subtracted from each electrode.

Data preprocessing was based upon the model shown in equation (1).[58] In this step, two corrections are applied to the raw EEG to deal with these distortions, as explained in a) and b):

a) multiplication by a random, general scale factor (GSF) ζ_i, specific for individual i,[58,63]
b) subtraction of the activity of the reference electrode $\beta_{i,j}(t)$.

This results in:

$$\mathbf{V}_{i.i}(t) = \zeta i\ \mathbf{V}^{raw}_{i.i}(t) - \beta_{i,i}(t)\ \hat{1}\beta_{i,i}(t), \qquad (1)$$

where $\hat{1}$ is the Nd vector of ones.

This model is based upon the assumption that all the time series are observations from stationary stochastic processes. In order to enable a tomographic analysis, which can describe spectral sources of the different frequencies without the need to consider interactions, it is desirable to construct a description in which the frequencies are independent. It has been shown[64] that under the above assumption, transformation to the frequency domain by the Fast Fourier Transform (FFT) (yielding a complex Gaussian distribution) is equivalent to a Principal Components Analysis which provides components that are independent by definition.

After the corrections defined above, the resulting $\mathbf{V}_{i,j}(t)$ were transformed to the frequency domain by means of the FFT, producing a set of complex vectors $\mathbf{V}_{i,j}(\omega)$. ω refers to frequency and varies from 1 to N_ω=49 (number of frequencies). These indexes correspond to the frequencies every 0.39 Hz, from 0.39 to 19.11 Hz, which is the bandwidth of the normative database presently used with VARETA. (Note that this limitation is not inherent in VARETA. In fact, the raw VARETA can be calculated for any frequency band-

width one selects. However, without a normative database with such bandwidth, the Z transform cannot be calculated, so Statistical Parametric Mapping cannot be provided.)

To accomplish tomographic mapping of the source spectra, it is first necessary to establish the interactions or covariances among all channels at each frequency, which can be calculated as a complex covariance matrix. By virtue of the central limit theorem," $\mathbf{V}_{i,j}(\omega)$ is distributed as a complex multivariate Gaussian vector that is statistically independent from the vectors at all other frequencies. This vector has zero mean and a complex symmetric (hermitic) covariance matrix $\sum_i(\omega)$, which is estimated by:

$$\mathbf{S}_i(\omega)=\frac{1}{Ne}\sum_{j=1}^{Ne}\mathbf{V}_{i,j}(\omega)\ \mathbf{V}_{i,j}(\omega)^*, \qquad (2)$$

where * denotes the conjugate transpose of a vector."

(Note: On occasion, it may be desirable to work directly with the cross-spectral matrix and not begin with the raw EEG. In that case, the corrections for the Global Scale Factor (GSF) and the reference electrode can be removed in a different way, as follows:

$$\mathbf{S}_i(\omega) = \frac{1}{\zeta_i^2}\mathbf{H}\bullet\mathbf{S}_i(\omega)\bullet\mathbf{H}, \qquad (3)$$

where H denotes the centering matrix[66] that transforms the data to the average reference[67] and the maximum likelihood estimate of the GSP is:

$$\zeta_i = \exp\left[\frac{1}{N_d\bullet N_\omega}\sum_{d=1}^{N_d}\sum_{\omega=1}^{N_\omega}\log\left(S_i^{dd}(\omega)\right)\right] \text{ where } S_i^{lm}(\omega) \text{ is}$$

the l,m entry in the cross spectral matrix, exp is the exponential function and fog is the natural logarithm.]

APPENDIX B

Frequency domain VARETA

Source EEG Inverse Solution

Based on the three concentric sphere model,[52] the forward problem of EEG may be specified in the frequency domain as follows:[31,32:69]

$$\mathbf{V}_i(\omega) = \mathbf{K}\bullet\mathbf{J}_i(\omega) + \mathbf{E}_i(\omega), \qquad (4)$$

where lhe magnitude $\mathbf{V}_i(\omega)$ denotes the true data and $\mathbf{E}_i(\omega)$ refers to error contributions from influences such as impedance fluctuations on the sensor array. $\mathbf{J}_i(\omega)$ represents the matrix of the x, y and Z components of the primary current field discretized on a grid inside the brain. In this work, the grid size was set to Ng=3623 points. K is the lead field matrix that relates current densities to observed measurements, which is obtained by spatial discretization.[39]

A complete treatment of the problem would require a discussion of how to select the reference. Following Pascual-Marqui et al (1994),[30] we have chosen to transform the data and the matrix K to the average reference.

The voxels for which primary currents must be estimated were defined by a grid placed in the volume of the brain. For VARETA using Me average MRI atlas, voxels were only included as specified by a mask identifying regions where the probability of gray matter was not zero, based upon the probabilistic brain tissue maps available from the Montreal Neurological Institute.

The usual objective of distributed EEG inverse solutions is to estimate the primary current field $\mathbf{J}_i$ from the data matrix V. This is the inverse *EEG problem for the source time series* and, as is well known, has no unique sol&n. The general VARETA inverse solution[31] for this problem is obtained by searching for those J that minimize the following objective function:

$$\sum_{ir=1}^{Ne}\Big((\mathbf{V}_{ir}(\omega) - \mathrm{K}\mathbf{y}\ \mathbf{J}_{ir}(\omega))^t \times \mathbf{S}_{\varepsilon_i}^{-1}(\omega) \times (\mathbf{V}_{ir}(\omega) - \mathrm{K}\mathbf{x}\ \mathbf{J}_{ir}(\omega)) + \mathbf{J}_{ir}(\omega)^t \times \mathbf{s}_{J_i}^{-1} \times \mathbf{J}_{ir}(\omega)\Big) + (m + N_e) \times \ln\left|\mathbf{S}_{ij}(\omega)\right| + \frac{1}{\tau_i^2(\omega)}\mathrm{Tr}\left\{\mathbf{s}_{J_i}^{-1}(\omega) \times \mathbf{G}\right\} \qquad (5)$$

where τ is the regularization parameter and $\mathrm{G} = (\Lambda_s \bullet \mathrm{L}_3^t \bullet \Lambda_m^2 \bullet \mathrm{L}_3 \bullet \Lambda_s)^{-1}$

This is a hierarchical generalization of the usual Bavesian formulation for inverse problems.[70] It should be noted that to minimize expression (5). the $\mathbf{J}_i(\omega)$ must be the outcome of a tradeoff between several factors:

1. $\sum_{r=1}^{N_{seg}}(\mathbf{V}_{ir}(\omega)-\mathbf{K}\bullet\mathbf{J}_{ir}(\omega))^t \bullet \Sigma_{\varepsilon_i}^{-1}(\omega)\bullet(\mathbf{V}_{ir}(\omega)-\mathbf{K}\bullet\mathbf{J}_{ir}(\omega))$

is just the usual measure of fit between the data and the model. $\sum_{Ei}$ is the covariance matrix of sensor noise.

2. $\sum_{r=1}^{N_{seg}}\mathbf{J}_{ir}(\omega)^t \bullet \Sigma_i^1(\omega)\bullet\mathbf{J}_{ir}(\omega)$ is a term that imposes lhe mask upon the solution which defines those voxels in which sources of the EEG are to be permitted. The source covariance $\sum_{Ji}(\omega)$ matrix specifies these assumptions.

3. The remaining term results from placing a natural conjugate prior[68] on $\sum_{Ji}(\omega)$ in which the a *priori* covariance matrix is proportional to G.

The purpose of G is to incorporate a number of assumptions about the sources which define the "regularization parameter":

- spatial smoothness is determined by $\mathbf{L}_3$, the Kronecker product of L with the identity matrix $\mathbf{I}_3$. L is any scalar roughness operator such as the discrete Laplacian or discrete thin plate spline operator. In this paper, the Laplacian operator is adopted as in Pascual-Marqui et al (1994).[30]
- the diagonal matrix Λ_s specifies the amount of smoothness to be applied at each point of the spatial grid. Large values of smoothing force constant solutions. Zero values specify no smoothing, i.e., a point solution.
- the diagonal matrix Λ_m defines Me a *priori* probability, obtained from the mask, that there might be any primary current density at a given location.

In this work. $\Lambda_m = \mathrm{W}\bullet\Lambda_G^{\frac{1}{2}}$, (6)

where W is the weight matrix introduced" to eliminate the

bias due to the greater sensitivity of observations to more superficial sources. The diagonal matrix Λ_G contains an estimate of the probability that there might be cortical gray matter for each point on the solution grid. These probabilities are available from the probabilistic tissue maps available at MNI.

In its most general form, the calculation of a VARETA estimate involves the use of the Expectation-Maximization (EM) Algorithm[72] in which $\tau_i(\omega)$ is estimated by minimizing the Generalized Cross-Validation Criterion (GCV).[68] Essentially, an estimate of the source spectra is obtained for each voxel and frequency by interpolation from the neighboring voxels and compared with the values actually allocated to that voxel. This nonlinear estimation procedure may achieve super resolution and eliminate 'ghost solutions" that are artifacts of simple linear inverse solutions.[44]

Source Cross-spectral Matrix Estimation

What has been described up to now is the estimation of the sources $J_i(\omega)$ for tomography. Topographic methods in Me frequency domain are based upon estimates of $\sum_i(\omega)$, *the source cross-spectrum.* An algorithmic simplification was introduced to allow the efficient estimation of this parameter. That simplification consists of substituting the data set $J_i(\omega) = [J_{i,1}(\omega), J_{i,2}(\omega), L, J_{i,N}(\omega)]$ for a given frequency by its statistical equivalent $S_i^{\frac{1}{2}}(\omega)$ in all calculations.

This statistical equivalent is the symmetric square root of the *estimate* of the "true EEG" *cross-spectrum defined* as $S_i^{\frac{1}{2}}(\omega) = \Psi_i(\omega) \bullet \text{diag}(\lambda_{i,j}^{\frac{1}{2}}(\omega)) \bullet \Psi_i^*(\omega)$, where $\Psi_i(\omega)$ is the matrix of eigen-vectors and $\text{diag}(\lambda_{i,j}^{\frac{1}{2}}(\omega))$ is the diagonal matrix of the square roots of the eigen-values of $S_i(\omega)$.

Wth this notation, the estimation procedure is as follow

Initialization: The procedure starts with an initial value for $\sum_i(\omega)$. To be specific:

$$\sum_{J_i}(\omega) = \Lambda_G \bullet W \bullet L_3^t \bullet \Lambda_G^2 \bullet L_3 \bullet W \bullet \Lambda_G \qquad (7)$$

Iteration: For the k-th step, the algorithm alternates between the two following steps:

$$1.\ A_{J_i}(\omega)^{(k)} = \hat{\sum}_{J_i}(\omega)^{(k-1)} \bullet K^t \bullet \left(K \bullet \hat{\sum}_{J_i}^{(k-1)} \bullet K^t + \sum_{E_i}(\omega) \right)^{-1} \bullet S_i^{\frac{1}{2}}(\omega)$$

$$2.\ \hat{\sum}_{J_i}(\omega)^{(k)} = \frac{N_e A_{J_i}(\omega)^{(k)} \bullet A_{J_i}(\omega)^{(k)} + \frac{1}{\tau_i^2(\omega)^2} G}{m + N_e} \qquad (8)$$

which are repeated until the estimates converge.

An important point to emphasize is that the use of either expressions (7) - (9) implies use of me *full cross-spectral matrix* of the date in order to obtain an estimate of the source cross-spectrum. It is therefore incorrect to attempt to fit sources by means of just the power spectra of me EEG data.

VARETA fitted for 9623 (N_g) voxels and 49 (N_ω) frequencies produced 177,527 log transformed source spectral values $s_{i,r,r}(\omega)$:

$$\log(s_{i,r,r}(\omega)) = \mu_r(\omega, age) + \varepsilon_{i,r}(\omega), \qquad (9)$$

where the population mean value for the log spectrum at voxel r, $\mu_r(\omega, age)$, is a (usually nonlinear) function of age. and the error term $\varepsilon_{i,r}(\omega)$ is assumed to be Gaussian with standard deviation $\sigma_r(\omega, age)$. Estimation of $\mu_r(\omega, age)$ was carried out by means of polynomial regression.?

The Z transform for the source spectrum of any voxel is defined as:

$$Z_{i,r,r}(\omega) = \frac{\text{Log}(s_{i,r,r}(\omega)) - \mu_r(\omega, age)}{\sigma_r(\omega, age)}, \qquad (10)$$

where $Z_{i,r,r}(\omega)$ is the Z transform of me source log spectrum for individual i and voxel r.

REFERENCES

1. Matousek M, Volavka J, Roubicek J, Roth Z. EEG frequency analysis related to age in adults. Electroencephalogr Clin Neurophysiol 1967; 23:162-167.
2. John ER, Karmel BZ, Corning WC, Easton P, Brown D, Ahn H, John M, Harmony T, Prichep L, Toro A, Gerson I, Bartlett F, Thatcher R, Kaye H, Valdés P, Schwartz E. Neurometrics: numerical taxonomy identifies different profiles of brain functions within groups of behaviorally similar people. Science 1977; 196:1383-1410.
3. John ER, Prichep LS, Easton P. Normative data banks and Neurometrics: basic concepts, methods and results of norm construction. In: Gevins AS, Rémond A (eds). Handbook of Electroencephalography and Clinical Neurophysiology. Amsterdam: Elsevier; 1967; 1:449-495.
4. Valdés P, Hernández JL, Biscay R, Valdés JL. Non linear QEEG analysis Electroencephalogr Clin Neurophysiol 1993; 87:S135.
5. Matousek M, Petersen I. Frequency analysis of the EEG in normal children and adolescents. In: Kellaway P, Petersen I. (eds). Automation of Clinical Electroencephalography. New York: Raven Press: 1973; 75-102.
6. John ER. Ahn H, Prichep LS, Trepetin M, Brown D, Kaye H. Developmental equations for the electroencephalogram. Science 1980; 210:1255-1258.
7. Duffy FH, Bartels PH, Burchfiel JL. Significance probability mapping. Electroencephalogr Clin Neurophysiol 1981; 51:455-462.
8. John ER, Prichep LS. Friedman J, Easton P. Neurometrics: computer assisted differential diagnosis of brain dysfunctions. Science 1988; 293:162-169.
9. Alvárez A, Pascual R, Valdés P. EEG development equations confirmed for Cuban school children. Electroencephalogr Clin Neurophysiol 1987; 67:330-332.

10 Swets JA. Measuring the accuracy of diagnostic systems. Science 1988; 240: 1285-1293.

11. Valdés-Sosa P, Valdés M, Carballo J, Alvárez A, Díaz G, Biscay R, Peréz MC, Szava S, Virues T, Quesada ME. QEEG in a public health system. Brain Topog 1992; 4:259-266.

12 Hughes JR, John ER. Conventional and quantitative electroencephalography in psychiatry. J Neuropsychiatry Clin Neurosci 1999; 11:190-208.

13 Chabot RJ, Orgill AA, Crawford G, Harris MJ. Serfontein G. Behavioral and electrophysiological predictors of treatment response stimulants in children with attention disorders. J ChildNeurology 1999;14:343-351.

14 Czobor P, Volavka J. Quantitative EEG effect of risperidone in schizophrenic patients. J Clin Psychopharm 1993; 13:332-342.

15 John ER. Prichep LS. Principles of neurometrics and neurometric analysis of EEG and evoked potentials. In: Niedermeyer E, Lopes da Silva F. (eds). Electroencephalography: Basic Principles, Clinical Applications and Related Fields. Baltimore: Williams and Wilkins; 1993; 989-1003.

16 Prichep LS, John ER, Essig-Peppard T, Alper KR. Neurometric subtyping of depressive disorders. In: Plasticity and Morphology of the CNS. M.T.P. Press, 1990.

17 Prichep LS. Mas F, Hollander E, Liebowitz M, John ER, Almas M, DeCaria CM, Levine RH. Quantitative electroencephalographic (QEEG) subtyping of obsessive compulsive disorder. Psychiat Res 1993; 50:25-32.

18 Prichep LS, Alper KR, Kowalik SC, Vaysblat L, Merkin HA, Tom M, John ER, Rosenthal MS. Prediction of treatment outcome in cocaine dependent males using quantitative EEG. Drug Alc Depend1999; 54:35-43.

19 Valdés-Sosa P, Biscay R, Galán L, Bosch J, Szava S, Virues T. High resolution spectral EEG norms for topography. Brain Topog 1990; 3:281-282.

20 Galán L, Biscay R, Valdés P, Neira L, Virues T. Multivariate statistical brain electromagnetic mapping. Brain Topog 1994; 7:17-28.

21 Szava S, Valdés P, Biscay R, Galán L, Bosch J, Clark I, Junenéz JC. High resolution quantitative EEG analysis. Brain Topog 1994; 6:211-219.

22 Biscay R, Galán L, Virues T, Valdés P, Neira L, Rojas J. Localization error in biomedical imaging. Comput Biol Med 1992; 22:277-286.

23 Pascual R, González S, Valdés PBR. Current source density estimations and interpretation based on the spherical harmonic Fourier expansion. J Neurosci 1988: 43.

24 Srinivasan R, Tucker D, Murias M. Estimates of the spatial nyquist of the human EEG. www.egi.com/spatial.sampling.pdf 1997.

25 Scherg M, von Cramon D. Two bilateral sources of the late AEP es identified by a spatio-temporal dipole model. Electroencephalogr Clin Neurophysiol 1985; 62: 32-44.

26 Scherg M, von Cramon D. Dipole source potentials of the auditory cortex in normal subjects and patients with temporal lobe lesions. In: Hoke M, Grandori F, Romani GL (eds). Advances in Audiology, Auditory Evoked Magnetic Fields and Electric Potentials. Basel: Karger; 1990; 6: 165-193.

27 Lehmann D, Michel CM. Intracerebral dipole sources of EEG FFT power. Brain Topog 1989; 2: 155-164.

26 Wang JZ, Williamson SJ, Kauffman L. Magnetic source images determined by lead-field analysis: the unique minimum-norm least squares estimation. IEEE Trans Siomed Engineer 1992;39:665-667.

29 Fuchs M, Wagner M, Wischmann HA, Dosell O. Cortical current imaging. AdvancBiomagnetism.97; 1993

30 Pascual-MarquiRD, Michel CM, Lehmann D. Low resolution electromagnetic tomography: a new method for localizing electrical activity in the brain. Int J Psychophysiol 1994; 18:49-65.

31 Valdés-Sosa P, Garcia F, Casanova R. Variable resolution electromagnetic tomography. In: Proc 10th Int Conf on Biomagnetism, BIOMAG. Santa Fe, New Mexico; 1996.

32. Valdés P, Casanova R, Aubert E., Riera J, Korin W, and Garcia F. Variable resolution electro magnetic brain tomography based upon an average brain atlas. In: Proc 10th Int Conf on Biomag netism, BIOMAG. Santa Fe, New Mexico; 1996.

33. Valdés-Sosa P, Riera J, Casanova R. Spatio temporal distributed inverse solutions. In: Proc 10th Int Conf on Biomagnetism, BIOMAG. Santa Fe, New Mexico; 1996.

34 Valdés-Sosa P. Quantitative electroencephalographic tomography. Electroencephalogr Clin Neurophysiol 1997; 103: 28. Abstract.

35 Phillips JW. MEG-based imaging of focal neuronal current sources. IEEE Trans Med Imag 1997; 16:338-348.

36. Mazziotta JC, Toga A, Evans AC, Fox P, Lancaster J. A probabilistic atlas of the human brain: theory and rationale for its developmentNeuroimage 1995; 2:89-101.

37 Dale 4 Sereno M. Improved localization of cortical activity by combining EEG and MEG with MRI cortical surface reconstruction: a linear approach. J Cognit Neurosci 1993; 5:162-176.

38. Valdés P, Riera J, Bosch J, Biscay R, González S, Grave de Peralta R, Pascual R. Methods and systems for three dimensional tomography of activity and connectivity of brain and heart electromagnetic waves generators. May1934 (US5307807).

39. Riera J, Aubert E, Valdés P, Casanova R, Lins 0. Discrete Spline Electro-Magnetic Tomography (DSPET) based on realistic neuronatomy. In: Proc 10th Int Cord on Biomagnetism, BIOMAG. Santa Fe, New Mexico. 1996.

40, Wagner M, Fuchs M, Wischmann AA, Drenckhahn R, Kohler T. Smooth reconstruction of cortical sources from EEG or MEG recordings. In: Proc 10thInt Conf onBiomagnetism, BIOMAG. Santa Fe, New Mexico; 1996.

41, Golub GH. Matrix Computations; 1989.

42, Worsley KJ, Marrett S, Neelin P, Evans AC. A unified statistical approach for determining significant signals in location and scale space images of cerebral activation. In: Myers R, Cunningham VG, Bailey DL, Jones T (eds). Quantification of Brain Function Using PET. San Diego: Academic Press; 1995; 327-333.

43 Kondacs A, Szabo M. Long-term intra-individual variability al the background EEG in normals. Clin Neurophysiol 1999; 110:1708-1716.

44 Lutkenhoner B, Greenblatt R, Hamalainen MS, Mosher J, Scherg M, Tesche C, Valdéz-Sosa P. Comparison between different approaches to the biomagnetic inverse problem: workshop report. In: Aine CJ, Okada Y, Stroink J, Swithenby SJ, Wood CC (eds). Biomag 96: Proc 10th Int Conf on Biomagnetism. Heidelberg: Springer Verlag; 2000.

45. Fernández-Bouzas A, Casanova R, Harmony T, Valdéz P, Aubert E, Silva J, Fernández T, Martinez-Lopez M, Garcia F, Bosch J, Marosi E, Bernard J, Rodriguez M. EEG frequency domain distributed inverse solutions in lesions. Electroencephalogr Clin Neurophysiol 1997; 103:195.

46. Fernández-Bouzas A, Harmony T, Bosch J, Aubert E, Fernández T, Valdés P, Silva J, Martinez-Lopez M. EEG source spectra in brain infarcts. Neuroimage 1998;7:660.

47. Fernández-Bouzas A, Harmony T, Bosch J, Aubert E, Fernández T, Valdés P, Silva J, Marosi E, Martinez-Lopez M, Casian G. Sources of abnormal EEG activity in the presence of brain lesions. *Clin Electroencephalogr 1999; 30:1-7.*

46. Prichep LS, John ER, Tom M. Localization of deep white matter lymphoma using VARETA: a case study. Clin Electroencephalogr 2001; 32: 62-66.

49. Evans AC, Collins DL, Mills SR, Brown ED, Kelly RL, Peters TM. 3D statistical neuroanatomical models from 305 MRI volumes. Proc IEEE-Nuclear Science Symposium and Medical Imaging Conference 1993; 95:1813-1817.

50. Evans AC, Collins DL, Neelin P, MacDonald D, Kamber M, Marrett TS. Three-dimensional correlative imaging: applications in human brain mapping. In: Thatcher R, Hallet M, Zeffiro T, John ER, Huerta M (eds). Functional Neuroimaging: Technical Foundations. San Diego: Academic Press, 1994; 145-161.

51. Collins DL, Neelin P, Peters RM, Evans AC Automatic 3D intersubject registration of MR volumetric in standardized Talairach space. J Comp Assist Tomog 1994; 18:192-205.

52. Hoke M, Lutkenhoner B, Pantev C. Comparison between different methods to approximate an area of the human head by a sphere. In: Hoke M, Grandori F, Romani GL (eds). Advances in Audiology, Auditory-Evoked Magnetic Fields and Electric Potentials. Basel: Karger; 1990; 165-193.

5.3. Muller TJ, Thome J, Chiaramonti R, Kierks T, Maurer K, Fallgetter AJ, Frolich L, Scheubeck M, Strik WK. A comparison of QEEG and HMPAO-SPECT in the clinical severity of Alzheimer's disease. Eur Arch Psychiat Clin Neurosci 1997; 247:259-263.

54. Picton TW. The recording and measurement of evoked potentials. Handbook of Clinical Neurophysiology. 2nd ed. Amsterdam: Elsevier; 1987; 23-40.

55. John ER. Neurometrics. In: Adelman G (ed). Encylopedia of Neuroscience. Boston: Birkhauser; 1987; 2:908-910.

56. Gasser T, Verleger R, Bacher P, Stroka L. Development of the EEG of school-age children end adolescents. I. Electroencephalogr Clin Neurophysiol 1988; 69:91-99.

57. Gasser T, Jennen-Steinmetz C, Sroka L, Verleger R, Mōcks J. Development of the EEG of school-age children adolescents. II. Topography. Electroencephalogr Clin Neurophysiol 1988; 69:100-109.

58. Valdés-Sosa P, Bosch J, Gray F, Hernández J, Riera J, Pascual R, Biscay R. Frequency domain models of the EEG. Brain Topog 1992; 309-319.

59. Rodin EA. Some problems in the clinical use of topographic EEG analysis. Clin Electroencephalogr 1991; 22:23-29.

60. Nagata K, Tagwa K, Hiroi S, Shishidc F, Uemura K. Electroencephalographic correlates of blood flow and oxygen provided by positron emission tomography in patients cerebral infarction. Electroencephalogr Clin Neurophysiol 1989; 72:16-30.

St. Grave de Peralta R. González-Andino SL, Lutkenhoner B. Figures of merit to compare inverse solutions. Brain Topog 1996; 9: 117-124.

62. Grave de Peralta R, Olaf H, González S, Vogt H, Michel C. Linear inverse solutions with optimal resolution kernels applied to the electromagnetic tomography. Human Brain Map 1997; 5: 454-467.

63. Hernández JL, Valdés P, Biscay R, Virues T, Szana S, Bosch J, Riquénes A, Clark I. A global scale factor in brain topography. Intern J Neuroscience 1995; 76:267-278.

64. Brillinger DR. Time Series Data Analysis and Theory; 1975.

65. Valdés-Sosa P. Statistical bases. In: Harmony T (ed). Functional Neuroscience: Neurometric Assessment of Brain Dysfunction in Neurolgical Patients. New Jersey: Lawrence Erlbaum; 1984; 3:141-254.

66. Mardia KV, Kent JT, Bibby JM. Multivariate Analysis. Lcndcn: Academic Press Inc.; 1979.

67. Katznelson RD. *Linear operators on* the multichannel date matrices. In: Nunez PL (ed). Electric Fields of the Brain. New York; Oxford University Press; 1981.

69. Hernández JL, Valdés P, Biscay R, Virues T, et al. A global scale factor in brain topography. Internat J Neurosci 1994; 76:267-278.

69. Casanova R, Valdés-Sosa P, Garcia FM, Szava S, Bosch J, Riquénes A. Clerk I. Frequency domain distributed inverse solution. In: Pmc 10th Int Ccnf on Biomagnetism, SIOMAG. Santa Fe, New Mexico; 1996.

70. Tarantola A. Inverse Problem Theory. Amsterdam: Elsevier Science Publishers; 1987.

71. George J S, Lewis P S, Schlitt HA, Kaplan L, Gorodnitski I, Wood CC. Strategies for source space limitation in tomographic inverse procedures. In: Proc 9th Int Conf Biomagnetism. Vienna, Austria; 1993.

72. Dempster AP, Laird NM, Rubin DS. Maximum likelihood from incomplete date via the EM-algorithm. J Royal Statist Soc 1977; Series B:1-38.

73. Grenander U, Miller MI. Representation of knowledge in complex systems. J Royal Statist Soc 1994; Series B:549-603.

74. Thompson PM, MacDonald D, Mega MS, Holmes CJ. Evans AC, Toga AW. Detection and mapping of abnormal brain structure with a probabilistic atlas of cortical surfaces. J Comp Assist Tomog 1997; 21:567-581.

75. Thompson PM, Toga AW. Detection, visualization and animation of abnormal anatomic structure with a deformable probabilistic brain atlas based on random vector field transformation (Invited Paper). Med Image Analysis 1997; 1:271-294.

Localization of Deep White Matter Lymphoma Using VARETA: A Case Study

Leslie S. Prichep, E. Roy John and MeeLee Tom

Key Words
Brain Lesions
Multimodal Brain Imaging
QEEG
source Localization
Variable Resolution Electromagnetic Tomography (VARETA)

ABSTRACT

Methods have recently bean proposed for localization of multiple brain sources of particular EEG frequencies recorded from the scalp, to identify their most probable neuroanatomical generators. This paper reports the accurate localization of a deep white matter lymphoma, using Variable Resolution Electromagnetic Tomography (VARETA). The accuracy of thii localization was confirmed by MRI studies. The patient was referred for a quantitative EEG evaluation, two weeks following an automobile accident, with no know loss of consciousness. mere was marked excess and asymmetry of frontal slow wave activity, with highly significant hypocoherence. Significant gradient shifts within the left hemisphere were also seen. Visual inspection of the EEG tracings revealed theta paroxysms in left dorsolateral and mesial frontal regions. The MRI revealed a large space-occupying lesion deep within the white matter of the left frontal lobe, with evidence of subependymal spread and significant surrounding vasogenic edema. Localization of the sources of the maximal QEEG abnormalities using VARETA was consistent with the lesion location seen in the MRI images. This case demonstrates that VARETA can achieve highly sensitive and accurate localization of sources of QEEG abnormalities which lie in the deepest brain regions.

INTRODUCTION

In the last several years, a number of methods have been described for the source localization of generators of EEG or evoked potentials recorded from the scalp. The initial efforts toward this goal were directed toward dipole source potential analysisin thetimedomain, applied to the brainstem auditory evoked potentials[1] and to cortical auditory evoked potentials.[2] Subsequently, attention was directed to the problem of localization of multiple sources in the frequency domain, enabling analysis of the generators of EEG rhythm.[3-6]

While the literature already contains a number of demonstrations of clinical application of such methodsforthe localization of epileptiiorm activity: cerebrovascular accidents and tumors,[8,9] an issue of major clinical relevance is the question whether such methods are necessarily restricted to sources in the cortical gray matter relatively near the surface of the brain, or whether meaningful results can be obtained in deep brain structures such as the thalamus. This paper reports successful localization of a deep white matter lymphoma in a single patient, with confirmation by MRI studies.

CASEHISTORY

The patient was a 66-year-old female who presented for electrophysiological examination to the Neurometric Evaluation Service (NES), Department of Psychiatry, New York University School of Medicine, two and a half weeks after being in a motor vehicle accident. The patient had no recall of thespacificsoftheaccident, but reported to have been mildly bruised. There was no report of loss of consciousness. Subsequent to the accident, the patient complained of a persistent headache, confusion, and memory problems. No abnormalities were found on conventional neurological examination, however, the patient was referred for an MRI evaluation and a quantitative EEG evaluation.

METHODS

EEG Acquisition and Analysis

Twenty minutes of eyes closed, resting EEG were recorded from 19 electrodes pasted on the scalp at positions corresponding to the International 10/20 Electrode Placement System.[10] In addition, EOG electrodes were placed diagonally above and below the orbit of the eye, for detection of eye movement artifact, a ground electrode placed upon the cheek and an EKG lead on the thorax. The recording was monopo-

Leslie S. Prichep, PhD, is the Associate Director of the Brain Research Laboratories and Associate Professor in the Department of Psychiatry, New York University School of Medicine, and a Research Scientist at the Nathan S. Kline Institute for Psychiatric Research, Orangeburg, NY. E. Roy John, PhD is the Director of the Brain Research Laboratories and Full-Professor in the Department of Psychiatry, New York University School of Medicine and a Research Scientist at the Nathan S. Kline Institue for Psychiatric Research, Orangeburg, NY. MeeLee Tom, MS, is an Assistant Research Scientist in the Brain Research Laboratories, Department of Psychiatry, New York University School of Medicine, and Manager of the Neurometric Evaluation Service.

Address correspondence and reprint requests to Dr. Leslie S. Prichep, Brain Research Laboratories, Dept. Psychiatry, 550 First Avenue, New York, NY 10016.

Email: leslie@BRL4.med.nyu.edu

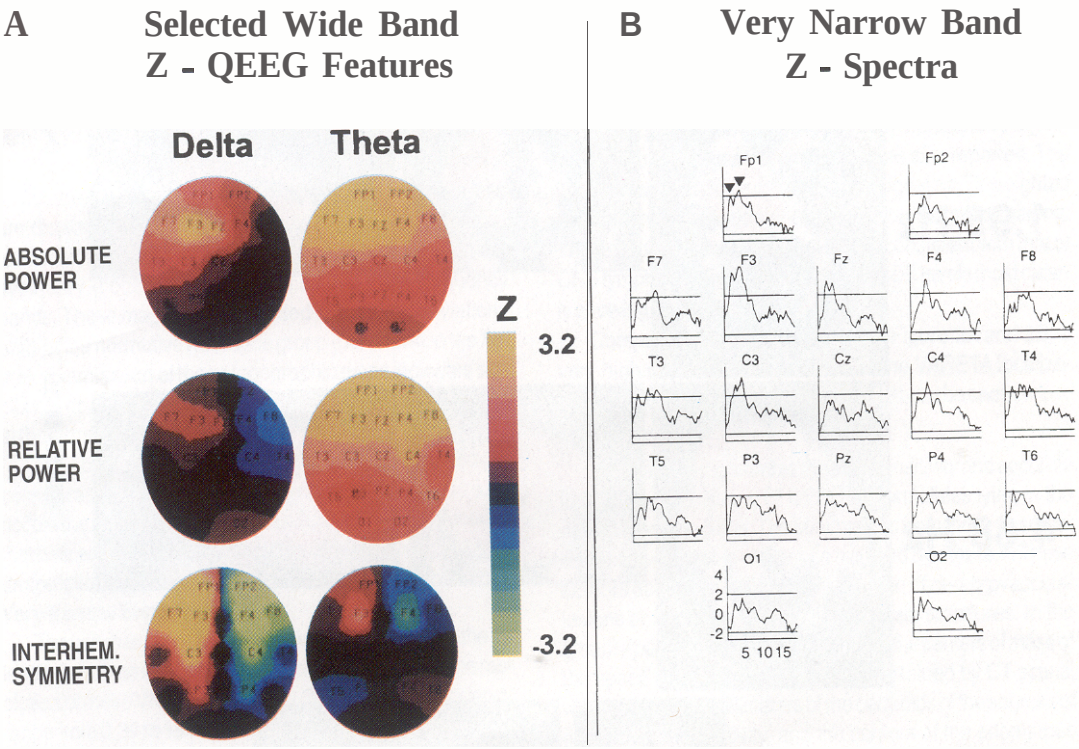

Figure **1A & 1B.**

A) Topographic QEEG Z maps of absolute power (top row), relative power (second row) and interhemispheric power symmetry (third row). These maps represent the difference between this patient and the expected normal values for her age, expressed in standard deviation of the normal group (not show" in the figure). Color coding is proportional to the Z-score. in, steps corresponding to those Show" on the Z scale, (range ±3.2). The center of the scale is normal (black), with shades of red to yellow indicating excess and blue to green indicating deficit. [Anterior is up and left on the left.]

B) The Very Narrow Band Z Spectra for each of the 19 scalp locations. Each panel represents the Z-spectra for that region, with a horizontal line at Z = 2.0 (P > 0.05). Show" at the Fp1 location (top left square) with ▼ are the frequency points selected for VARETA imaging from these spectra.

lar, referential to linked earlobes. Amplifiers had a bandpass from 0.5 to 70 Hz (3 dB points), with a 60 Hz notch filter. All impedances were kept below 5000 ohms, checked regularly throughout the procedure. The ND converter sampled at 200 Hz per channel, with 12-bit resolution. The data were reduced to 100 Hz prior to analysis, using a resampling algorithm which minimizes aliasing. This data acquisition was performed using a Cadwell Spectrum 32.

Afier visual editing to remove artifacts, 46 artifact free samples were selected, each 2.5 seconds long, for quantitative analysis. Significant test-retest reliability of samples of this length has been confirmed.[11] These data were then submitted for neurometric QEEG analysis.[12] Fast Fourier Transforms (FFTs) were performed on every segment in each channel. Average values across the 46 segments were obtained for a large number of quantitative spectral features, including absolute and relative power in the delta (1.5-3.5 Hz), theta (3.5-7.5 Hz), alpha (7.5-12.5 Hz) and beta (12.5-20 Hz), as well as the inter- and intra-hemispheric coherence and symmetry between regions for the same frequency bands. Data were log transformed for Gaussianity and age-regressed.[13,14] Standard or Z-scores were then computed for each of these measures, using the mean values and standard deviations of the normative distributions from the neurometric database for each.

RESULTS

Wide Band Neurometric Findings

There were highly significant abnormalities ($P < 0.001$) seen in the QEEG analysis, including: [1] excesses of absolute power in delta in left frontal regions, maximal at F3; [2] excesses of absolute and relative delta activity over frontal and central regions in both hemispheres; [3] increased mean frequency in delta in the left frontal and central regions; [4] slow wave asymmetries between frontal regions and between central regions, with more power on the left than the right hemisphere; [5] gradient shifts in slow waves within the left hemisphere between anterior and posterior regions with more power in the

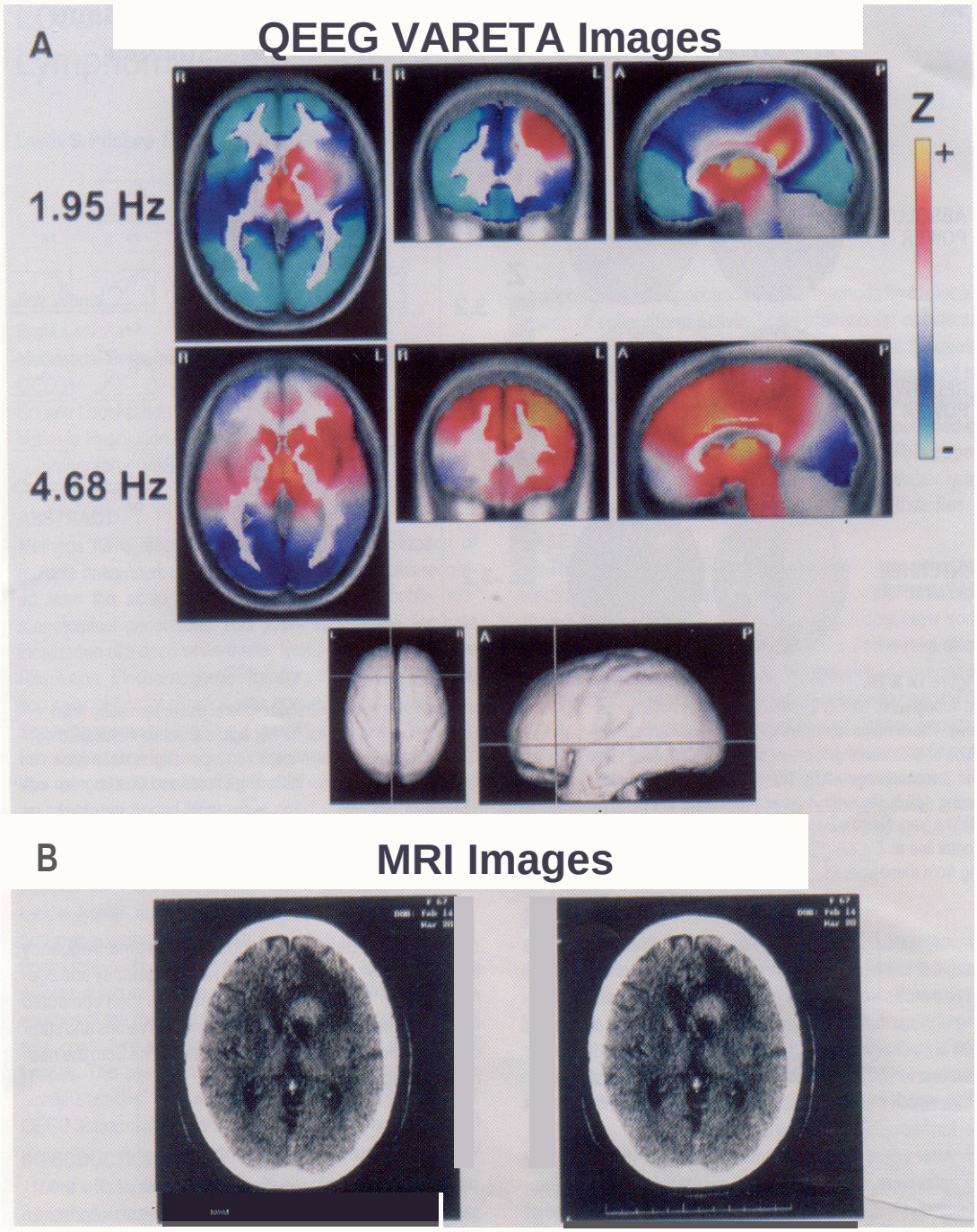

Figure 2A & B.
A) QEEG VARETA 3D images at two different narrow-band frequencies. At each frequency the VARETA images of transaxial, sagittal and coronal sections are shown at levels shown in the schematic (third row). The top row is at 1.96 Hz and the second row is at 4.68 Hz. Color coding is in standard deviation unit.3 of the normals, not shown in this figure. with white representing the center of the scale, shades of red to yellow showing increasing excess and green showing increasing deficit. The Z scale range is ±1.0 for the first row of images and ±3.0 for the second row. These images follow radiologic convention, laterality is reversed.
B) Selected slices from the MRI evaluation of this patient.

anterior regions; [6] hypocoherence in slow waves between left and right frontal regions, between central regions, between posterior temporal regions and between parietal regions. Visual inspection of the EEG record revealed theta paroxysms in left dorsolateral and mesial frontal regions.

Topographic interpolated head maps of Z-scores for selected features showing the most prominent abnormalities are displayed in Figure 1 A, including absolute power (top row), relative power (middle row) andinterhemispheric power symmetry (bonom row) for the delta and theta frequency bands. These maps are color coded in standard deviations units of the normative reference group (not shown in the figure). Examination of these topographic maps indicates significant departures from expected normative values. Colors at the extremes indicate $P < 0.001$.

The abnormal QEEG findings did not correspond to our considerable experience with patients after mild head injury, nor did the multivariate profile of abnormalities correspond to thatdefined by statistical descriptors of post-concussion syndrome following mild head injury, described by us[12] or others.[15]

Very Narrow Band Findings

The very narrow band (VNB) power Z-spectra from the 19 leads were examined and are illustrated in Figure1 B. The resolution of these VNB spectra was 0.39 Hz over the frequency range from 0.39 to 19 Hz. The VNB frequencies at which the largest Z-scores were found (significant differences from expected normal value for age) were ascertained to be at approximately 1.96 Hz and 4.66 Hz. These two points are marked with a ▼ at Fp1 in Figure1 B. An asymmetry of significant delta excess can be seen, with higher Z values on anterior regions on the left side. The theta peak, while largest on the left side, spreads across the midline in the F4 and C4 regions.

Variable Resolution Electromagnetic Tomography Findings

The two most abnormal frequencies from the Z VNB spectra (described above) were 1.96 Hz and 4.68 Hz. Using Variable Resolution Electromagnetic Tomography (VARETA), the sources of these abnormalities were sought. VARETA identifies the most probable underlying sources of the scalp recorded EEG, estimated by means of a discrete spline EEG inverse solution,[8] (Bosch-Bayard et al, this volume). Anatomical constraints are incorporated by the use of the Montreal Neurological Institute (MNI) probabilistic brain atlas.[16] The VARETA results are depicted in Figure 2A. The source of the delta activity (top row) was attributed to a relatively focal deep source, shifted to the left side. The theta source (second row) was less focal, also deep and maximal on the left.

MRI Findings

The MRI indicated a large abnormal enhancing mass lesion within the deep white matter of the left frontal lobe with evidence of subependymal spread about the margins of the left ventricular system as well as the right frontal horn. Significant surrounding vasogenic edema was also reported. The lesion was noted to have decreased signal on T2 weighted imaging and increased signal on diffusion weighted imaging. These findings were considered to be consistent with that of CNS lymphoma. Figure 2B shows the MRI levels most clearly showing thelesion.

Comparing the images shown in Figure 2A and 2B, a very high correspondence between the VARETA localization of maximal abnormality and the MRI can be seen.

DISCUSSION

This case demonstrates the high sensitivity and accurate localization of sources of QEEG abnormalities lying in the deepest brain regions. The conclusions from these observationsarecompatible with those reached by others.[8,9] These authors described VARETA localization of cerebrovascular lesions or tumors in many different brain structures. In the group of patients which they described, the centers of mass of the space occupying lesions, as ascertained by CT scans, were within a few millimeters of the centroids of the sources of excessive delta activity, and the centers of the edematous surrounds of the lesions were close to the centroids of the theta excesses.

We suggest that the delta excesses around the tumor in the present case arose due to compression of neural tissue (at the level of the *thalamus)* by the expanding tumor volume. The source of the theta excess was more diffuse, most probably reflecting the edema at the margins of the tumor. The correct location of the sources which served as the generators of the salient neurometric QEEG abnormalities provides support for the belief that valid VARETA images can be constructed for generators in deep brain regions and are not a priori restricted to sources near the surface of the cortex.

These findings demonstrate the potential clinical utility of QEEG and VARETA analysis for a preliminary identification of such brain abnormalities. This has important implications for clinical use due to the availability and cost effectiveness of EEG evaluations as compared with MRI and other more invasiveimaging methods.

DEDICATION

This paper is dedicated to the memory of RB.

REFERENCES

1. Scherg M, von Cramon D. Two bilateral sources of the late AEP as identified by a spatio-temporal dipole model. Electroencephalogr Cli" Neurophysiol 1985; 62: 3244.
2. Scherg M, von Cramon D. Dipole source potentials of the, auditory cortex in normal subjects and patients with temporal lobe lesions. In: Hoke M, Grandori F, Romani GL (eds). Advances in Audiology, Auditory Evoked Magnetic Fields and Electric Potentials. Basel: Karger; 1990; 6:165-193.
3. Pascual-Marqui RD. Michel CM, Lehmann D. Low resolution electromagnetic tomography: a new method for localizing electrical activity in the brain. Int J Psychophysiol 1994; 18: 49-65.
4. Grave de Peralta R, Olaf H, González S, Vogt H, Michel C. Linear inverse solutions with optimal resolution kernels applied to the electromagnetic tomography. Human Brain Map 1997; 5:454-467.
5. Valdés-Sosa P, Garcia F, Casanova R. Variable resolution electromagnetic tomography. In: Wood C (ed). Proceedings of the 10th International Conference on Biomagnetism. Santa Fe, New Mexico: 1996.
8. Bosch-Bayard J, Valdés-Sosa P, Virues-Alba T, Aubert-Vázquez E, John ER, Riera-Díaz J, Trujillo-Barreto N. 3D statistical parametric mapping of EEG source spectra by means of variable resolution electromagnetic tomography (VARETA). Clin Electroencephalogr 2001; 32: 47-61.
7. Ebersole JS, Pacia SV. Localization of temporal lobe foci by ictal patterns. Epilepsia 1996; 37: 386-399.
8. Fernández-Bouzas A, Casanova R, Harmony T, Bosch J, Aubert E, Fernández T, Valdés P, Silva J, Marosi E, Martinez-Lopez M. EEG frequency domain distributed inverse solutions in lesions. Electroencephalogr Clin Neurophysiol 1997; 103: 195.
9. *Fernández-Bouzas* A, *Harmony T*, Bosch J, *Aubert-Vázquez* E, Fernández T, Valdés P, Silva J, Marosi E, Martinez-Lopez M, Casian G. Sources of abnormal EEG activity in the presence of brain lesions. Clin Electroencephalogr 1999; 30: 1-7.
10. Jasper HH. The 10/20 electrode system of the International Federation of Electroencephalography. Electroencephalogr Clin Neurophysiol 1958; 10: 371.375.
11 Kondacs A, Szabo M. Long-term intra-individual variability of the background EEG in normals. Clin Neurophysiol 1999; 110: 1708-1716.
12 John ER, Prichep LS. Principles of neurometrics and neurometric analysis of EEG and evoked potentials. In: Niedermeyer E, Lopes da Silva F (eds). Electroencephalography: Basic Principles, Clinical Applications and Related Fields. Baltimore: Williams and Wilkins. 1993; 989-1003.
13 John ER, Ahn H, Prichep LS, Trepetin M, Brown D, Kaye H. Developmental equations for the electroencephalogram. Science 1980; 210: 12551258.
14 Gasser T, Bacher P, Mochs J. Transformation towards the normal distribution of broadband spectral parameters of the EEG. Electroencephalogr Clin Neurophysiol 1982; 53: 118124.
15 Thatcher RW, Walker RA, Gerson I, Geisler FH. EEG *discriminant analyses of mild head trauma. Electroencephalogr Clin* Neurophysiol 1989; 73: 94-106.
16 Evans AC, Collins DL, Mills SR, Brown ED, Kelly RL. Peters TM. 3D statistical neuroanatomical models horn 305 MRI volumes. Proc IEEE-Nuclear Science Symposium and Medical Imaging Conference. London: M.T.P. Press 1993; 95: 1813-1817.